Electron acceleration by few-cycle laser pulses with single-wavelength spot size

G. I. Dudnikova,[1] V. Yu. Bychenkov,[2] A. Maksimchuk,[3] G. Mourou,[3] J. Nees,[3] S. G. Bochkarev,[2] and V. A. Vshivkov[1]
[1]*Institute of Computational Technologies, Novosibirsk, Russia*
[2]*P.N. Lebedev Physics Institute, Moscow, Russia*
[3]*Center for Ultrafast Optical Science, University of Michigan, Ann Arbor, Michigan 48109*
(Received 18 September 2002; published 27 February 2003)

Generation of relativistic electrons from the interaction of a laser pulse with a high density plasma foil, accompanied by an underdense preplasma in front of it, has been studied with two-dimensional particle-in-cell (PIC) simulations for pulse durations comparable to a single cycle and for single-wavelength spot size. The electrons are accelerated predominantly in forward direction for a preplasma longer than the pulse length. Otherwise, both forward and backward electron accelerations occur. The primary mechanism responsible for electron acceleration is identified. Simulations show that the energy of the accelerated electrons has a maximum versus the pulse duration for relativistic laser intensities. The most effective electron acceleration takes place when the preplasma scale length is comparable to the pulse duration. Electron distribution functions have been found from PIC simulations. Their tails are well approximated by Maxwellian distributions with a hot temperature in the MeV range.

DOI: 10.1103/PhysRevE.67.026416 PACS number(s): 52.38.Kd, 52.35.Mw, 52.75.Di

I. INTRODUCTION

The fast ignitor scheme, high-energy electron injectors, and x-ray sources have triggered a worldwide interest to generate relativistic electron bunches. A remarkable result is laser-produced electron jets in the interaction of ultraintense light pulses with solid targets at tens to hundreds of joules of laser energies [1–4]. As tabletop lasers continue to reach record levels of peak power, they also can be used to accelerate beams of electrons to several MeV energies with millijoule laser energy scale at a kilohertz repetition rate [5]. Further improvements will allow these compact lasers to be useful as hard radiation sources for cancer radiotherapy, electron injectors, ultrashort point-size x-ray sources, and tools for nuclear physics, chemistry, and biology on the femtosecond time scale and on the spatial scale of atoms.

Because of the finite laser energy contrast ratio, the interaction of laser pulses with solid targets is typically characterized by preplasma formation before the peak of the pulse reaches the target. Such a preplasma is a reason for enhanced electron generation providing a plethora of mechanisms for electron acceleration. These electrons can be accelerated up to several MeV energies due to several processes, such as, stimulated forward Raman scattering [6], resonant absorption [7], laser wake fields [8], ponderomotive acceleration by standing [9], and propagating [10] laser pulses, ''vacuum heating'' due to the $\mathbf{v}\times\mathbf{B}$ component of the Lorentz force [11] or the Brunel effect [12], wave breaking of self-modulated laser wake fields [13], injection via coupling of Raman-backscattered radiation to the plasma wake [14], and betatron resonance provided by laser-pulse channeling [15]. Clearly, a better understanding of the mechanisms of electron acceleration in the interaction of the ultrashort ultrafocused laser pulses with solid targets and quantification of the electron beam characteristics in terms of laser pulse and the plasma parameters is essential for the success of new applications of tabletop lasers.

In this paper, we report on the results of a fully relativistic two-dimensional (2D) particle-in-cell (PIC) simulation of fast particle generation in the interaction of ultrashort laser pulses with dense targets with preplasma conditions. Electron acceleration with preplasma is different as compared to both extended homogeneous plasmas and dense plasma slabs with sharp boundaries. The study of possible regimes of electron acceleration by short relativistic laser pulses in plasma coronas is still incomplete. The aim of this paper is to focus on the aspect of electron generation in short preplasma of the size of several laser wavelengths by relativistic laser pulses consisting of only a few optical cycles. We consider a focused spot radius of only one laser wavelength.

These conditions are met by the chirped pulse amplification laser at the Center of Ultrafast Optical Science (CUOS), as illustrated by Fig. 1. This indirectly diode-pumped Ti:Sapphire laser works at 1-kHz repetition rate and has the advantage of being stable (1%), compact (on a single $8'\times10'$ table), highly intense (few times of 10^{18} W/cm^2) at a rather low-energy level (<3 mJ) and relatively low cost. Further improvement of this installation will allow interaction with plasma at strongly relativistic intensities, $I=10^{19}$ W/cm^2.

We study here the mechanisms of electron acceleration for the conditions described. For preplasmas several laser wavelengths thick, which can be attributed to moderate to

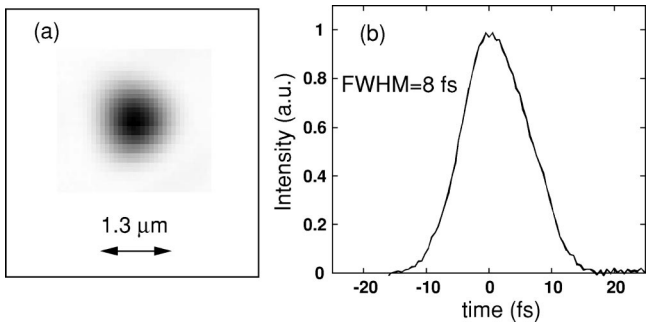

FIG. 1. Spatial and temporal characteristics of CUOS 1-kHz repetition rate laser: focal spot size (a) and pulse duration (b).

low prepulse energy, only a few mechanisms of acceleration of the electrons rather than the enumerated ones are most likely. We confirm the result of Ref. [16] for longer laser pulse duration, that the energy of the electron entering the target from preplasma scales linearly with intensity at relativistic laser fields, $a>1$, where a is the dimensionless amplitude of the laser vector potential. However, with ultrashort laser pulses the mechanism of electron acceleration is different. In Ref. [10], a rare preplasma with density much lower than critical has been considered, and electron acceleration was attributed to the propagating laser pulse abruptly stopping at the target surface, so that the highly energetic electrons within the pulse continue to move forward inertially and escape from the pulse in the forward direction. This mechanism is also present here but is inhibited because of the high preplasma density responsible for collective plasma phenomena.

We found that the most effective mechanism of electron acceleration originates from the electrostatic self-induced electric field behind the short laser pulse. This field accelerates electrons and they even overtake the laser pulse. This is accompanied by breaking of the formed electron wave that terminates further acceleration of the electrons. The stochastic behavior of electron motion due to wave breaking produces a Maxwellian-like hot electron distribution. When the laser pulse reaches the dense foil, the high-energy electron bunch penetrates through the target and escapes behind it. We have investigated the efficiency of electron acceleration versus the laser and plasma parameters and found optimum conditions for energetic electron production. Normal incidence laser pulses have been considered. We demonstrated that several MeV electrons can be triggered by relativistic intensities few-cycle laser pulses of millijoule energy both in forward and backward directions.

The paper is organized as follows. In Sec. II, we describe the PIC model and demonstrate two qualitatively different regimes of electron acceleration in forward (1) and both forward and backward (2) directions. In Sec. III, we describe the mechanisms of electron acceleration. The efficiency of electron acceleration versus plasma and laser parameters are studied in Sec. IV. We conclude with a summary in Sec. V.

II. ELECTRON DISTRIBUTIONS FROM ULTRASHORT LASER-PULSE INTERACTION WITH FOIL

Two-dimensional PIC simulations with total number of particles 10^6 and 32 particles per cell were performed for linearly polarized laser pulses with a wavelength λ_0 propagating normally to a plasma target (hydrogen) in the x direction of the X-Y simulation plane.

This target models a thin solid dense plasma slab of thickness $0.25\lambda_0$ positioned at $x=12\lambda_0$ and having a rare plasma in front of it to model the blow-off plasma created by the laser prepulse that interacts with the foil before the main pulse reaches the target. The dense plasma slab has electron density n_e 40 times higher than the critical density n_c. The total simulation box is $17.5\lambda_0\times 17.5\lambda_0$. The preplasma is at $x>2\lambda_0$ with electron density $0\leqslant n_e\leqslant 1.3n_c$ of an exponential profile with a spatial scale length L. This profile was truncated near the plasma-vacuum boundary to have $n_e=0$ at $x=2\lambda_0$. The laser pulse propagates in x direction from left to right with vacuum electric field amplitude E_{y0} and frequency ω_0. It has $d=2\lambda_0$ focal size. The position of the laser beam axis corresponds to $y=8.8$. The boundary conditions for particles, electric and magnetic fields are periodic in y direction. In x direction, they consist of electromagnetic wave that enters the region $x>0$ and freely leaves the computational domain at the right boundary. Particles reflect from the boundaries in the x direction. Plasma consists of protons and electrons with ion mass $m_i=1836m_e$. The simulations were performed for normalized amplitudes of the laser vector potential, $a=eE_{y0}/mc\omega_0=2,4,7$, and 14 where c is the speed of light, e is the electron charge, and m is the electron mass. These values correspond to the intensities from $I_0=8.6\times 10^{18}$ to 4.2×10^{20} W/cm^2 for laser light with wavelength 0.8 μm. There was a $2\lambda_0$ vacuum layer before the plasma target and significantly longer vacuum region behind to reduce boundary effects. The laser-pulse length l was in the range $1.5\lambda_0<l<6\lambda_0$ and the preplasma density gradient scale was chosen $2\lambda_0<L<6.5\lambda_0$. Anywhere below, the coordinates, time, momenta, and energies are given in λ_0, $2\pi/\omega_0$, mc, and mc^2, correspondingly.

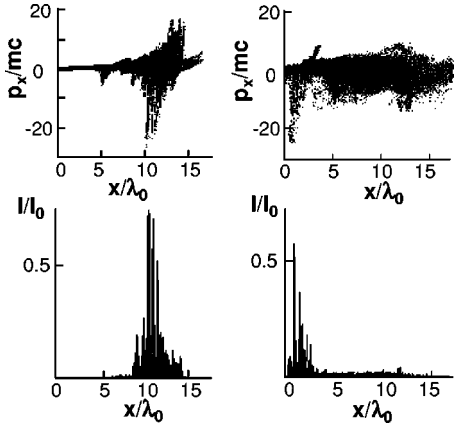

FIG. 2. The electron phase space plots $x-p_x$ at $t=15$ and $t=24$ (left and right upper panels, correspondingly) for $a=7$, $l=3$, and $L=2$. Intensity of the electromagnetic field for the same time intervals (left and right bottom panels, correspondingly).

An underdense plasma in front of the target even with the size of few laser wavelengths is crucial to high-energy electron generation. Simulations demonstrate acceleration of electrons in such underdense preplasma. Figures 2 and 3 illustrate production of electron jets in forward and backward directions. The mechanism of electron acceleration in forward direction is discussed in the following section. The forward-accelerated electrons escape from the region behind the incident laser pulse when it reflects and they pass through the foil target. As the laser pulse propagates backwards after reflection, it accelerates a small number of electrons to energies that can be even higher than that of the forward electrons, as shown on the right panel of Fig. 2. The strong backward acceleration can be attributed to the relativistic return-current electrons escaping from dense plasma even before the reflected pulse catches them. Having higher initial momenta they are accelerated by the laser pulse to higher

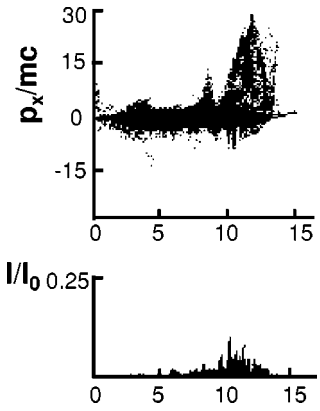

FIG. 3. The electron phase space plot $x-p_x$ at $t=16$ (upper panel) for $a=7$, $l=3$, and $L=5$. Normalized intensity of the electromagnetic field, I, for the same time moment (bottom panel).

energies than the electrons in forward direction. While the electron bunch in the forward direction is always observed, the electron jet in the backward direction is not generated in a thick preplasma because of the low intensity of the reflected pulse in this case (Fig. 3). One concludes from this result that a better quality electron injector for the backward direction can be achieved only with a high-intensity contrast ratio when the preplasma is short enough.

The PIC model gives details of the electron energy distributions. A typical example is presented in Fig. 4 for $a=7$ and for laser-pulse lengths comparable to (left panel) or longer than (right panel) the characteristic preplasma size L. Electron distribution functions consist of the thermal electron bulk and hot electron tails well approximated by Maxwellian distributions with effective temperatures, shown in Fig. 4 over the curves. The bulk of ''cold'' electrons are generated from both the dense plasma foil and the preplasma, while the hot component represents only electrons accelerated in the preplasma. For a preplasma scale length shorter than the laser-pulse width, an electron from the preplasma cannot acquire an energy comparable to the quiver energy corresponding to the laser peak intensity. Conversely, this *is* the case for shorter laser pulses with the duration comparable to or shorter than L. This is why for $L/l\sim 1$ the effective fast electron production in the forward direction is possible when the propagating laser pulse is abruptly stopped at the target surface allowing the highly energetic electrons to continue moving inertially. This is clearly seen from comparison of the left and right panels in Fig. 4 where for the same laser

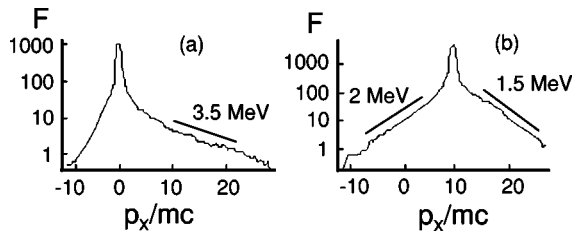

FIG. 4. The electron distribution functions for $a=7$, $l=6$, $t=16$, and $L=2$ (right panel) and $L=5$ (left panel) with and without backward-accelerated electrons, correspondingly.

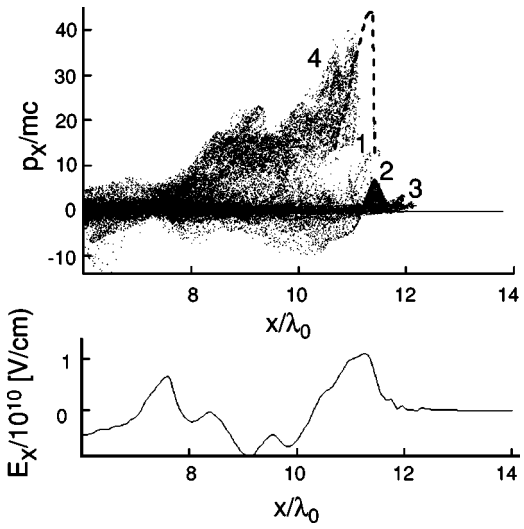

FIG. 5. The electron phase space plot $x-p_x$ at $t=20$ (upper panel) for $a=7$, $l=3$, and $L=6.5$. Position of laser pulse is shown by dashed curve in the upper panel. The numbers enumerate the different groups of electrons. The spatial distribution of average electrostatic e field (bottom panel).

intensity the forward-accelerated electrons in preplasmas with characteristic scale lengths comparable to laser-pulse duration have 2.5 times higher average energy than the same electrons accelerated in small scale preplasmas ($L<l$). The left panel in Fig. 4 also illustrates the effect mentioned above, which is the suppression of backward electron acceleration in the case of an extended plasma corona. In the extended preplasma, the laser pulse experiences higher absorption mainly due to the generation of hot electrons [1]. Its scattering in the preplasma is also higher. Neither effect provides a significant reflected pulse at the target surface, and consequently, effective backward electron acceleration is prevented.

III. MECHANISMS OF ELECTRON ACCELERATION

In Fig. 5, the simulation results for the spatial distribution of the longitudinal electron momentum p_x averaged over the y, and the longitudinal component of electric field in a plasma with $L=6.5$ and $l=3$ are shown shortly prior the pulse reaches the critical density surface. Four different groups of electrons accelerated in the preplasma can be identified.

Group 1. These are electrons within the laser pulse. The pulse carries them to the foil and they escape from the laser pulse when it hits the foil target. These electrons were studied in Ref. [10]. For the conditions of current interest (dense preplasma and short laser pulse), these accelerated electrons do not contribute significantly to the entire population of hot electrons.

Group 2. The pulse pushes the preplasma electrons similar to a snowplow (Fig. 5). These electrons are concentrated at the front side of the pulse. They have less energy than the electrons within the pulse but their density, shown in Fig. 6, is much higher. The electrons of group 2 form, in fact, a solitary electrostatic wave that moves with the group veloc-

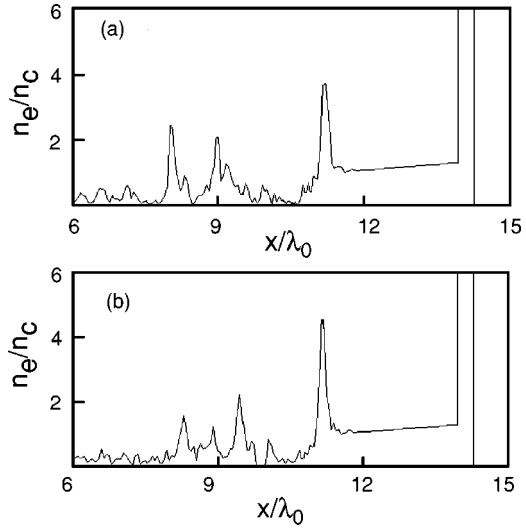

FIG. 6. Electron density in n_c units at $t=20$ for $a=7$, $l=3$, and $L=6.5$ at $y=8.6$, (a) and at $y=8.8$ (b).

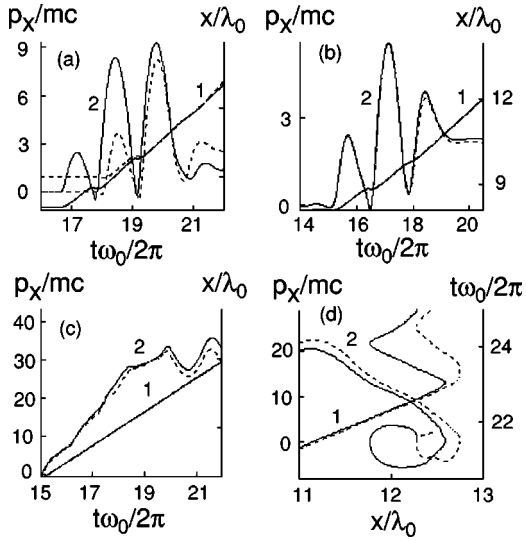

FIG. 7. The momenta (2) and x coordinates (1) of two particles (solid and dashed lines, correspondingly) from the group 2 (a), group 3 (b), and group 4 (c), (d).

ity of laser pulse, which decreases while laser pulse penetrates into a plasma. This solitary wave is stable, however, the average electron energy within it experiences oscillations. Being pushed outward by the laser pulse, the electrons produce a positive charge separation electrostatic field within the laser pulse, which acts as a deceleration force for the electrons behind the laser-pulse front. This electric field has a maximum at the laser beam axis and its magnitude reaches $0.5a$. A similar quasistationary solitary wave has been demonstrated in 1D PIC simulation [17]. In our 2D case, it looks like a semihoop at the laser-pulse head [cf. panels a and b in Fig. 6] with electron density maximum at the laser axis, $y=8.8$. The perturbation of density in the electrostatic wave is several times (up to four to five times) higher than the background density. The width of this structure is extremely small, only half of a laser wavelength. In Fig. 7(a), the results of tracing representative electrons are shown to identify their nature. The momenta of these group 2 electrons oscillate [Fig. 7(a)] showing that they are captured at the laser-pulse front. Their trajectories show that the electrons are displaced with average velocity close to the group velocity of the laser-pulse.

Group 3. The electrons of this group lead the laser-pulse front (Fig. 5). They are expelled from the laser pulse and move inertially in accordance with Fig. 7(b). Oscillations of p_x in Fig. 7(b) demonstrate, indeed, that the repelled electrons had been traveling with the pulse before they left it. Electron momentum finally saturates when electrons leave the pulse. It was demonstrated in Ref. [18] that for a circular polarized laser pulse traveling with the group velocity lower than the speed of light, the electrons can be repelled if a corresponding threshold is exceeded. This threshold reduces with laser-pulse group velocity decrease. The same takes place for a linearly polarized laser pulse. Although the analytic solution of the Lorenz equations for a single electron interacting with a given linearly polarized laser pulse is unknown, we found it numerically for a Gaussian laser pulse and a defined repelling threshold similar to the approach of Ref. [18]. This result is presented in Fig. 8, where two kinds of particles are clearly seen, repelled electrons and electrons overtaken by the laser pulse. The distance required for electrons to be repelled versus the laser-pulse group velocity is also shown in Fig. 8. Qualitatively, the $p_x(t)$ dependence of repelled electrons corresponds to the PIC simulations. Quantitative comparison is not straightforward because of the inhomogeneity of group velocity and collective plasma effects, in particular, due to the strong decelerating electrostatic field that reduces the energy of expelled electrons significantly compared to test particles for a given laser-pulse shape. However, this result sheds light on the nature of the electrons discussed and demonstrates that for characteristic group velocity $v_g \approx 0.7-0.8$ corresponding to Fig. 5 the distance $\sim 2\lambda_0$ is enough for the electrons to be expelled.

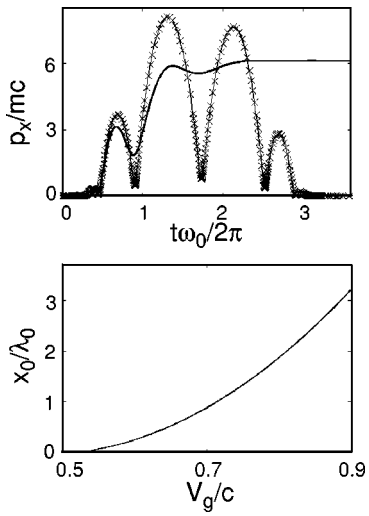

FIG. 8. Evolution of the longitudinal momentum of a single electron initially at rest in the Gaussian linearly polarized laser pulse with $a=4$ and $l=3$ (upper panel) and the distance x_0 required for an electron to be repelled vs the laser-pulse group velocity (bottom panel). The group velocity in the upper panel is chosen 0.85 (solid line) and 0.95 (line with markers).

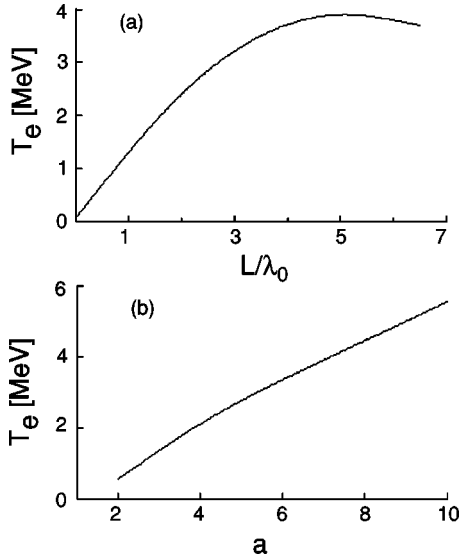

FIG. 9. The hot electron temperature dependencies of forward-accelerated electrons on preplasma size L [$a=7$, $l=3$, panel (a)] and laser field amplitude a [$L=5$, $l=3$, panel (b)].

Group 4. Electrons with maximum energy are formed behind the laser pulse (Fig. 5). They are accelerated by the high negative electrostatic field created by ponderomotive evacuation of the electrons within the laser pulse. The latter is clearly demonstrated by $p_x(t)$ for representative electrons of group 4 in Fig. 7(c). Significant numbers of the electrons being accelerated by the strong electrostatic field overtake the laser pulse. The momentum $p_x(t)$ increases nearly linearly with time until these particles overtake the laser pulse because their velocity becomes higher than the pulse group velocity. This corresponds to oscillations of $p_x(t)$ in Fig. 7(c) at time $t>20$. Similar to group 2 electrons, these electrons look like a well formed bunch of high-energy electrons [17,19,20]. The corresponding density perturbation is presented in Fig. 6 just behind the laser pulse. It is much wider than the front density perturbation and strongly modulated in time and in the transverse direction [cf. Figs. 6(a) and 6(b)]. While the average density of this bunch is lower than the density of the front electron bunch, its energy is significantly higher. This electron wave similar to the front wave moves with a velocity close to the group velocity of the laser pulse. Simulations demonstrate that the structure discussed experiences wave breaking at later times. Corresponding electron trajectories are shown in Fig. 7(d). When electrons reach the backside of the pulse, they experience decelerating electric field. However, electron energy does not drop strongly because the laser pulse is reflected when it hits the target surface and the high-energy particles continue to move forward inertially, penetrating through the foil.

The tracing performed allows us to identify the hot electrons generated in forward direction in the tail of the distribution function (Fig. 4) as consisting of those particles accelerated by an electrostatic field in the preplasma behind the laser pulse (group 4). These particles form a jet at the rear side of the foil, which is characterized by a small angular spread. The bulk of the electron distribution is formed by the particles accelerated from the foil, and the moderate energy

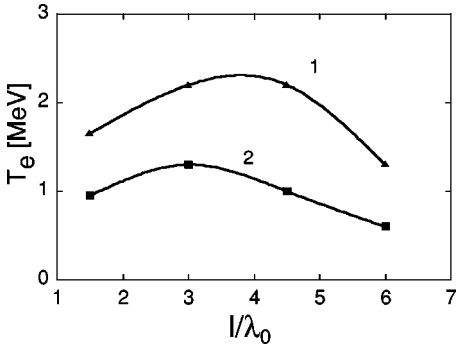

FIG. 10. The hot electron temperature dependencies on pulse duration, l for $a=4$ and $L=5$ (1) and $L=2$ (2).

part of the distribution between the tail and the bulk originates from the semihoop solitary wave at the laser-pulse front (group 2). Penetrating through the foil, these electrons produce a nearly isotropic distribution. Their spatial distribution looks like a halo surrounding a hot electron jet (see below Fig. 13).

IV. ELECTRON ACCELERATION DEPENDING ON PLASMA PARAMETERS

Our simulations demonstrate that target design is a crucial issue for electron acceleration. Both characteristic preplasma size and laser-pulse length influence electron energy. We have found that at the same laser intensity, hot electron energy reaches maximum if the preplasma size is comparable to the pulse length, $L\sim(1-2)l$. The dependencies of hot electron temperature on the preplasma scale length in Fig. 9 (upper panel) and on the pulse duration in Fig. 10 show this. For a thin preplasma layer, electrons cannot be well accelerated and their energies grow with L. On the other hand, for extended preplasmas $L\gg l$ particle mixing due to wave breaking and laser-pulse losses lead to the lowering of average electron energy. This is why both $T_e(L)$ and $T_e(l)$ dependencies in Figs. 9 and 10 demonstrate smooth maxima.

The hot electron temperature dependence on a is shown in Fig. 9 (bottom panel). Electron temperature grows linearly with a in accordance with relativistic scaling [16]. Indeed, the potential difference produced by relativistic electrons accelerated by the leading edge of the laser pulse scales with the ponderomotive potential, $\propto a$, so also does the energy of electrostatically accelerated electrons behind the laser pulse. Note that there is an indication of such scaling, $T_e\propto I_0^{1/2}$, in the experiments of Ref. [21]. We also quantified the dependence of number of several MeV electrons on the laser field amplitude as shown in Fig. 11. More than 10^9 of several MeV electrons can be generated by $\sim$10-fs pulses with a total laser energy of several millijoules.

Simulations performed demonstrate also that the efficiency of hot electron production depends on preplasma scale length. The electron phase space plot before laser-pulse reflection is shown in Fig. 12 for a preplasma with a density profile having a plateau at low density. Comparison to the similar case (Fig. 2) without preplasma density tailoring shows a fourfold increase of maximum electron energy for the same laser intensity and pulse duration. The spatial dis-

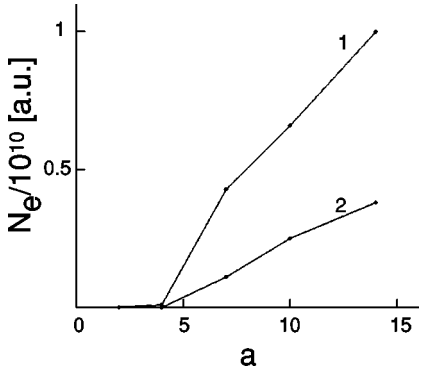

FIG. 11. The number of hot electrons, N_e, with energy exceeding 5 and 10 MeV (lines 1 and 2, correspondingly).

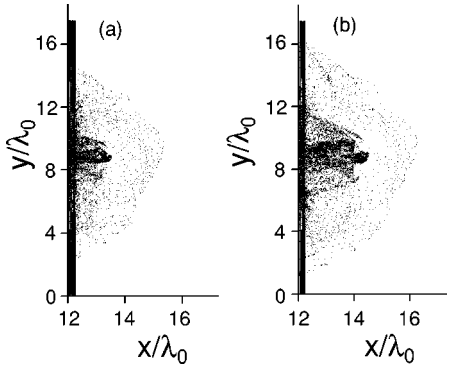

FIG. 13. Spatial distribution of accelerated electrons behind the foil just after they leave the target (a) and some later (b) for the same parameters as in Fig. 12.

tribution of the electrons escaping from the target is shown in Fig. 13 demonstrating a hot electron jet due to electrostatic acceleration and a halo from a semihoop solitary electron wave formed at the laser-pulse front. We believe that preplasma density profiling will aid experiments aimed at improving the acceleration properties by coherent control.

V. CONCLUSIONS AND SUMMARY

In this paper, we have performed PIC simulations of electron acceleration triggered by relativistic laser pulses consisting of only a few optical cycles and focusing to a spot of only one laser wavelength. High-energy electrons originate from the interaction of laser pulses with preformed plasma in front of an overdense plasma slab. Such preformed plasmas likely appear in most experiments because of nonideal laser-pulse contrast. The results give evidence that a preplasma of size of several wavelengths leads to enhanced generation of hot electrons.

From the simulations described we inferred two Maxwellian-like electron distributions with hot electron temperature having a linear dependence on laser intensity. We found that the characteristic preplasma size influences the efficiency of electron generation. For preplasmas longer than the laser-pulse length, the electrons are accelerated predominantly in the forward direction. For preplasma thickness shorter than or comparable to the laser-pulse length, both forward and backward accelerations of electrons take place. The highest electron energy is achieved for preplasma size comparable to the laser-pulse length. Tailoring of the plasma density profile is an effective way to increase electron energy.

When a relativistic laser pulse propagates through a thin preplasma it forms a dense bunch of electrons at the leading edge of the pulse with density higher than the critical density. This solitonlike plasma structure penetrates through the foil and forms the bulk of the distribution function of forward-accelerated electrons. More energetic tails of the electron distribution behind the foil originate from the electrons ac-

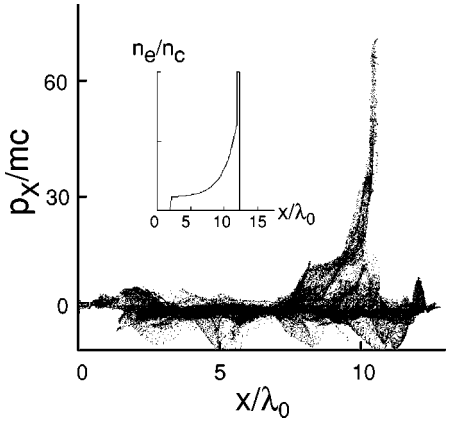

FIG. 12. The electron phase space plot $x-p_x$ shortly before laser-pulse reflection for $a=7$ and $l=3$ for the tailored density profile shown as inset.

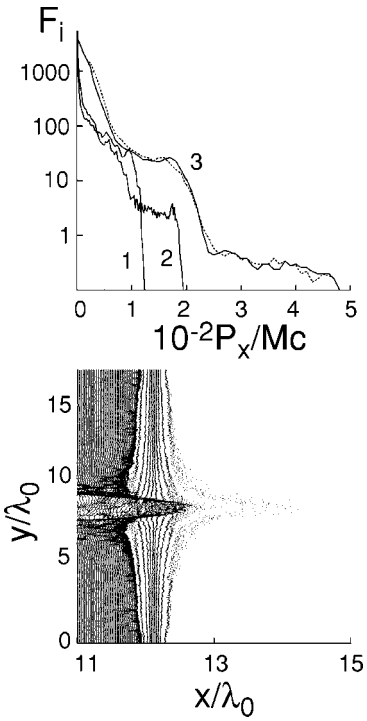

FIG. 14. The ion energy distribution functions (upper panel) for $a=7$, $l=6$, and $L=5$ at $t=12$ (1), 17 (2), 37 (dashed line), and 47 (3). The time $t=12$ corresponds to electron penetration in the foil. Spatial distribution of accelerated ions behind the foil at $t=47$ (bottom panel).

celerated by Coulomb fields generated at the trailing edge of the laser pulse. These electrons have several times higher energy but lower density. This electrostatic mechanism of electron acceleration is found to be the major effect responsible for hot electron generation by ultrashort laser pulses in such thin preplasma layers.

It is well known that fast electron production is an origin of effective ion acceleration [22] and hence two groups of hot electrons just mentioned above should produce similar groups of ions. Figure 14 illustrates this by two plateaus in ion energy distribution (upper panel) and two corresponding jets in ion density distribution (bottom panel).

Because ions are much heavier than electrons, a quite long time is needed to accelerate them [23]: $\sim M/en_h$, where n_h is the hot electron density. This is why for ultrashort laser pulses, considered in this paper, proton acceleration occurs when laser pulse is already reflected and has left plasma. The ion maximum energy saturates with time at the value [16] $\sim T_h$ that approximately corresponds to the momentum cutoff in Fig. 14.

A kilohertz repetition rate laser with the capability of delivering pulses of a few optical cycles in a wavelength-scale focus and at relativistic intensities currently exists at the Center for Ultrafast Optical Science at the University of Michigan. It is coupled with a target system that allows millions of shots on a single target while supplying fresh target surface for each shot. To the best of our knowledge, measurements of x-ray spectrum and spot size as well as optical effects and particle acceleration are possible in this wavelength-cubed regime.

ACKNOWLEDGMENTS

This work was partly supported by the Russian Foundation for Basic Research (Grant No. 00-02-16063), INTAS (Grant No. 2002-233), and the National Science Foundation (Grant ''FOCUS''). Two of us, V.Yu.B. and G.I.D., acknowledge the sponsorship of the regents of the University of Michigan and the Center for Ultrafast Optical Science. We thank D. V. Romanov for assistance in figure preparation.

[1] M.H. Key, M.D. Cable, T.E. Cowan, K.G. Estabrook, B.A. Hammel, S.P. Hatchett, E.A. Henry, D.E. Hinkel, J.D. Kilkenny, J.A. Koch, W.L. Kruer, A.B. Langdon, B.F. Lasinski, R.W. Lee, B.J. MacGowan, A. MacKinnon, J.D. Moody, M.J. Moran, A.A. Offenberger, D.M. Pennington, M.D. Perry, T.J. Phillips, T.C. Sangster, M.S. Singh, M.A. Stoyer, M. Tabak, G.L. Tietbohl, M. Tsukamoto, K. Wharton, and S.C. Wilks, Phys. Plasmas **5**, 1966 (1998); K.B. Wharton, S.P. Hatchett, S.C. Wilks, M.H. Key, J.D. Moody, V. Yanovsky, A.A. Offenberger, B.A. Hammel, M.D. Perry, and C. Joshi, Phys. Rev. Lett. **81**, 822 (1998).

[2] P.A. Norreys, M. Santala, E. Clark, M. Zepf, I. Watts, F.N. Beg, K. Krushelnick, M. Tatarakis, A.E. Dangor, X. Fang, P. Graham, T. McCanny, R.P. Singhal, K.W.D. Ledingham, A. Creswell, D.C.W. Sanderson, J. Magill, A. Machacek, J.S. Wark, R. Allott, B. Kennedy, and D. Neely, Phys. Plasmas **6**, 2150 (1999); M.I.K. Santala, M. Zepf, I. Watts, F.N. Beg, E. Clark, M. Tatarakis, K. Krushelnick, A.E. Dangor, T. McCanny, I. Spencer, R.P. Singhal, K.W.D. Ledingham, S.C. Wilks, A.C. Machacek, J.S. Wark, R. Allott, R.J. Clarke, and P.A. Norreys, Phys. Rev. Lett. **84**, 1459 (2000).

[3] L. Gremillet, F. Amiranoff, S.D. Baton, J.-C. Gauthier, M. Koenig, E. Martinolli, F. Pisani, G. Bonnaud, C. Lebourg, C. Rousseaux, C. Toupin, A. Antonicci, D. Batani, A. Bernardinello, T. Hall, D. Scott, P. Norreys, H. Bandulet, and H. Pepin, Phys. Rev. Lett. **83**, 5015 (1999).

[4] R. Kodama, K.A. Tanaka, Y. Sentoku, T. Matsushita, K. Takahashi, H. Fujita, Y. Kitagawa, Y. Kato, T. Yamanaka, and K. Mima, Phys. Rev. Lett. **84**, 674 (2000).

[5] O. Albert, H. Wang, D. Liu, Z. Chang, and G. Mourou, Opt. Lett. **25**, 1125 (2000).

[6] C.D. Decker, W.B. Mori, and T. Katsouleas, Phys. Rev. E **50**, 3338 (1994).

[7] S.C. Wilks and W.L. Kruer, IEEE J. Quantum Electron. **33**, 1954 (1997).

[8] T. Tajima and J.M. Dawson, Phys. Rev. Lett. **43**, 267 (1979).

[9] S.C. Wilks, W.L. Kruer, M. Tabak, and A.B. Langdon, Phys. Rev. Lett. **69**, 1383 (1992).

[10] Wei Yu, V. Bychenkov, Y. Sentoku, M.Y. Yu, Z.M. Sheng, and K. Mima, Phys. Rev. Lett. **85**, 570 (2000).

[11] W.L. Kruer and K. Estabrook, Phys. Fluids **28**, 430 (1985).

[12] F. Brunel, Phys. Rev. Lett. **59**, 52 (1987).

[13] A. Modena, Z. Najmudin, A.E. Dangor, C.E. Clayton, K.A. Marsh, C. Joshi, V. Malka, C.B. Darrow, C. Danson, D. Neely, and F.N. Walsh, Nature (London) **377**, 606 (1995).

[14] E. Esarey, C.B. Schroeder, W.P. Leemans, and B. Hafizi, Phys. Plasmas **6**, 2262 (1999).

[15] A. Pukhov, Z.-M. Sheng, and J. Meyer-ter-Vehn, Phys. Plasmas **6**, 2847 (1999).

[16] Y. Sentoku, V.Yu. Bychenkov, K. Flippo, A. Maksimchuk, K. Mima, G. Mourou, Z.M. Sheng, and D. Umstadter, Appl. Phys. B: Lasers Opt. **B74**, 207 (2002).

[17] A. Zhidkov, M. Uesaka, K. Kinoshita, and J. Koga, in 2002 IEEE International Conference on Plasma Science, 2002 (unpublished), Abstracts, p. 112.

[18] C.J. McKinstrie and E.A. Startsev, Phys. Rev. E **54**, 1070 (1996).

[19] T.V. Liseikina, F. Califano, V.A. Vshivkov, F. Pegoraro, and S.V. Bulanov, Phys. Rev. E **60**, 5991 (1999).

[20] I. Dudnikova, V.Yu. Bychenkov, Z. Chang, A. Maksimchuk, G. Mourou, J. Nees, and V.A. Vshivkov, Bull. Am. Phys. Soc. **46**(8), 26 (2001).

[21] A.G. Zhidkov, A. Sasaki, I. Fukumoto, T. Tajima, T. Auguste, P. D'Oliveira, S. Hulin, P. Monot, A.Ya. Faenov, T.A. Pikuz, and I.Yu. Skobelev, Phys. Plasmas **8**, 3718 (2001).

[22] S.J. Gitomer, R.D. Jones, F. Begay, A.W. Ehler, J.F. Kerhart, and R. Kristal, Phys. Fluids **29**, 2679 (1986).

[23] V.Yu. Bychenkov, Y. Sentoku, S.V. Bulanov, K. Mima, G. Mourou, and S.V. Tolokonnikov, Pis'ma Zh. Eksp. Teor. Fiz. **74**, 664 (2001) [JETP Lett. **74**, 586 (2001)].